Publications

7-10-2004

Proper Motion Objects in the Hubble Deep Field

M. Kilic
University of Texas at Austin

Ted von Hippel
University of Texas at Austin, vonhippt@erau.edu

et al.

Follow this and additional works at: https://commons.erau.edu/publication

Part of the Stars, Interstellar Medium and the Galaxy Commons

PROPER MOTION OBJECTS IN THE HUBBLE DEEP FIELD[1]

M. KILIC AND TED VON HIPPEL

University of Texas at Austin, Department of Astronomy, 1 University Station C1400, Austin, TX 78712; kilic@astro.as.utexas.edu, ted@astro.as.utexas.edu

R. A. MENDEZ

European Southern Observatory, Casilla 19001, Santiago, Chile; rmendez@eso.org

AND

D. E. WINGET

University of Texas at Austin, Department of Astronomy, 1 University Station C1400, Austin, TX 78712; dew@astro.as.utexas.edu

Received 2004 January 31; accepted 2004 March 25

ABSTRACT

Using the deepest and finest resolution images of the universe acquired with the *Hubble Space Telescope* and a similar image taken 7 yr later for the Great Observatories Origins Deep Survey, we have derived proper motions for the point sources in the Hubble Deep Field–North. Two faint blue objects, HDF 2234 and HDF 3072, are found to display significant proper motion, 10.0 ± 2.5 and 15.5 ± 3.8 mas yr^{-1}. Photometric distances and tangential velocities for these stars are consistent with disk white dwarfs located at ~ 500 pc. The faint blue objects analyzed by Ibata et al. and Mendez & Minniti do not show any significant proper motion; they are not halo white dwarfs, and they do not contribute to the Galactic dark matter. These objects are likely to be distant active galactic nuclei.

Subject headings: dark matter — Galaxy: halo — stars: evolution — white dwarfs

1. INTRODUCTION

Major observational campaigns have searched for dark matter in the form of massive compact halo objects (MACHOs) using microlensing events (e.g., Alcock et al 1997; Afonso et al. 2003; Udalski et al. 1992). The detection of 13–17 microlensing events toward the Large Magellanic Cloud over a period of 6 yr by the MACHO collaboration implies that a significant fraction (20%) of the halo of the Galaxy may be in the form of compact halo objects (Alcock et al. 2000). The timescale of these lensing events eliminates the possibility of MACHOs having substellar masses. The MACHO collaboration finds a most probable mass of 0.5 $M_\odot$, which supports the idea of a massive halo composed of baryonic matter in the form of low-luminosity white dwarfs (Kawaler 1996). Recent observations by the EROS group provide further evidence that less than 25% of a standard dark matter halo can be composed of objects with a mass between 2×10^{-7} $M_\odot$ and 1 $M_\odot$ (Afonso et al. 2003).

Halo white dwarf stars are expected to have large proper motions as a result of their high velocities relative to the Sun. *Hubble Space Telescope* (*HST*) proper motion studies of the globular cluster NGC 6397 showed that most of the required dark matter in the solar vicinity can be accounted for by a population of old white dwarfs representing the thick disk and halo of the Galaxy (Mendez 2002). Claims by Oppenheimer et al. (2001) and Ibata et al. (2000) that they had found a significant population of halo white dwarfs from kinematic surveys are tantalizing. Their discoveries seemed to be consistent with earlier findings of an old population of white dwarfs in the Hubble Deep Field (HDF; Mendez & Minniti

2000). However, further analysis by several groups showed that the sample of Oppenheimer et al. (2001) could also be interpreted as the tail of a kinematically warmer white dwarf component, better explained by the thick disk population of the Galaxy (Reid et al. 2001; Reyle et al. 2001; Mendez 2002; Bergeron 2003).

The HDF provides a unique window on the universe (Williams et al. 1996; Flynn et al. 1996). The extreme depth of the HDF provides an unprecedented opportunity to find faint stellar objects as well as to study very distant galaxies. The advantage of going deep is that it allows us to search for faint stellar components of the Galaxy in the regions of the color-magnitude diagram that are devoid of any contamination by standard Galactic stars. The lack of ordinary disk stars is due to the finiteness of the Galaxy (Flynn et al. 1996). Mendez & Minniti (2000) claimed that the faint blue objects found in the Hubble Deep Field–North (HDF-N) and Hubble Deep Field–South (HDF-S) are Galactic stars, based on the observed number of blue sources and extragalactic sources in the two fields. Independent proper motion measurements for five of these faint blue sources by Ibata et al. (1999) suggested that they are cool halo white dwarfs, which could account for the entire missing mass in the solar neighborhood. Third-epoch data on these five objects, however, did not show any significant proper motion (R. Ibata 2003, private communication; Richer et al. 2001).

We use the original HDF-N data and images of the same field taken 7 yr later for the Great Observatories Origins Deep Survey (GOODS) to measure proper motions of the point sources analyzed by Ibata et al. (1999) and Mendez & Minniti (2000).

2. PROPER MOTION MEASUREMENTS

GOODS is a multiwavelength, multifacility deep survey designed to study galaxy formation and evolution over a large redshift range. It includes deep imaging with the Advanced

TABLE 1
Point Sources in the Hubble Deep Field

Object	X(HDF)[a]	Y(HDF)[a]	X(GOODS)[b]	Y(GOODS)[b]	V	$V-I$
HDF 2272	869.387	989.094	3952.627	838.889	19.78	1.04
HDF 2234[c]...........	2903.711	1129.655	6500.462	8114.658	20.78	0.20
HDF 101	315.227	3788.366	4778.925	4538.35	21.45	1.12
HDF 1583	1026.935	1803.079	4580.210	1742.69	22.19	1.47
HDF 1828	2448.822	1573.769	6184.354	704.792	24.30	2.38
HDF 3072[c]...........	1877.251	349.952	4837.550	7714.658	24.27	1.29
HDF 2134	1194.967	1255.044	4489.335	987.877	24.74	2.52
HDF 2258	247.806	1117.993	3264.773	1328.88	24.95	2.91
HDF 1470	2440.850	1935.845	6368.745	1148.24	25.33	1.50
HDF 1481	3424.519	1920.592	7554.512	601.04	25.87	2.22
HDF 161	1388.682	3818.963	6098.469	4001.02	25.74	0.77
HDF 684	956.369	2845.424	5052.038	3049.25	26.70	1.82
HDF 3031[c]...........	3380.128	403.175	6688.739	6975.563	26.50	0.44
HDF 759	534.482	2774.917	4501.172	3190.23	26.66	0.46
HDF 3000[c]...........	1306.869	420.559	4178.915	8105.979	27.36	3.19
HDF 995	642.304	2475.111	4471.563	2767.75	27.08	0.52
HDF 1022	401.701	2504.499	4195.475	2932.52	27.87	0.29
HDF 861	537.648	2643.861	4434.536	3028.95	27.87	0.06
HDF 1705	2113.471	1690.358	5839.241	1025.76	28.11	0.46
HDF 2729	1746.126	710.752	4866.870	31.945	28.30	0.70
HDF 2217	2766.571	1181.931	6359.981	59.073	28.26	0.34
HDF 806[d]............	1171.947	2699.015	5235.329	2756.72	28.57	0.61
HDF 1135	1064.710	2306.869	4895.408	2337.47	28.78	1.16
HDF 2991	291.521	436.858	2951.714	479.141	28.58	0.24
HDF 1288	926.550	2096.186	4613.698	2154.15	28.53	−0.07
HDF 946	351.213	2538.371	4151.918	2999.19	28.49	−0.37
HDF 1196	1030.595	2279.031	4839.458	2321.74	28.79	0.74
HDF 723	938.652	2806.484	5008.853	3012.2	28.92	0.94
HDF 1816[d]...........	3006.002	1601.085	6874.624	438.659	29.02	0.45
HDF 1039	593.115	2432.467	4388.899	2741.84	28.43	−1.35
HDF 774	445.116	2747.477	4378.614	3204.48	28.82	0.03

Notes.—There is an offset between our coordinates and the GOODS Teams r1.0 version of the source catalogs (Giavalisco et al. 2004). The offset is +300 pixels in X and +200 pixels in Y.
[a] Chip coordinates from the HDF mosaics.
[b] Chip coordinates from GOODS section 33.
[c] Chip coordinates from GOODS section 32.
[d] Object in common with Ibata et al. (1999).

Camera for Surveys (ACS) in the B, V, i, and z bands, and reaches down to AB = 28.1, 28.4, 27.7, and 27.6 in the four bands, respectively (10 σ, point source; Giavalisco et al 2003). Our second-epoch data, acquired with *HST* and ACS as part of the GOODS ACS Treasury program, provide a baseline of 7 yr. The GOODS team released version 1.0 of the reduced, calibrated, stacked, and mosaicked images of the HDF-N in 17 sections. Section 32 (total integrations of 34.9 ks in V and 36.9 ks in I) and section 33 (48.9 ks in V and 51.9 ks in I) overlap with the original HDF-N images.

The source catalogs for the first epoch are produced by the Space Telescope Science Institute (STScI) from the combined and drizzled images. We note that the first-epoch HDF-N catalog is based on rereduced HDF-N images by Casertano et al. (2000), providing a 10% increase in depth. We used the SExtractor package (Bertin & Arnouts 1996), version 2.3, to build source catalogs from the second-epoch data. The major motivation for using SExtractor was its incorporation of weight maps in modulating the source detection thresholds. Source detection was carried out on the inverse-variance–weighted sum of the V- and I-band drizzled images. The combined $V + I$ image is deeper than any of the individual images (Casertano et al. 2000). Only those objects matching the positions of the objects in the first-epoch data with differences less than 0″.2

are included in our final catalog. Furthermore, we visually inspected all of the sources used for our proper motion study to avoid any mismatches. Although the GOODS Team released version 1.0 of the ACS multiband source catalogs, their catalogs are based on z-band detection only (M. Giavalisco et al. 2004, in preparation). Hence, the released catalogs are not appropriate for the study of faint blue objects. The GOODS data are 0.5–0.8 mag shallower than the original HDF images; therefore, we use the first-epoch images for photometry. Astrometric and photometric data for the point sources in the HDF-N are given in Table 1. We adopted the calibrated V and I photometry of Mendez & Minniti (2000).

Although the effective point-spread function (ePSF) fitting procedure (Anderson & King 2000) is the most precise astrometric technique for *HST* images, well-exposed star images are required to accurately sample the PSF. There are not many stars in the HDF, and the main source of error in our proper motion measurements is the positions of the reference compact objects (galaxies). Therefore, the ePSF method is not necessary and was not used for our analysis.

The original HDF images were rereduced and corrected for distortion by Casertano et al. (2000). The second-epoch data were corrected for distortion by the GOODS team using the latest (2003 July) coefficients released by the ACS group at
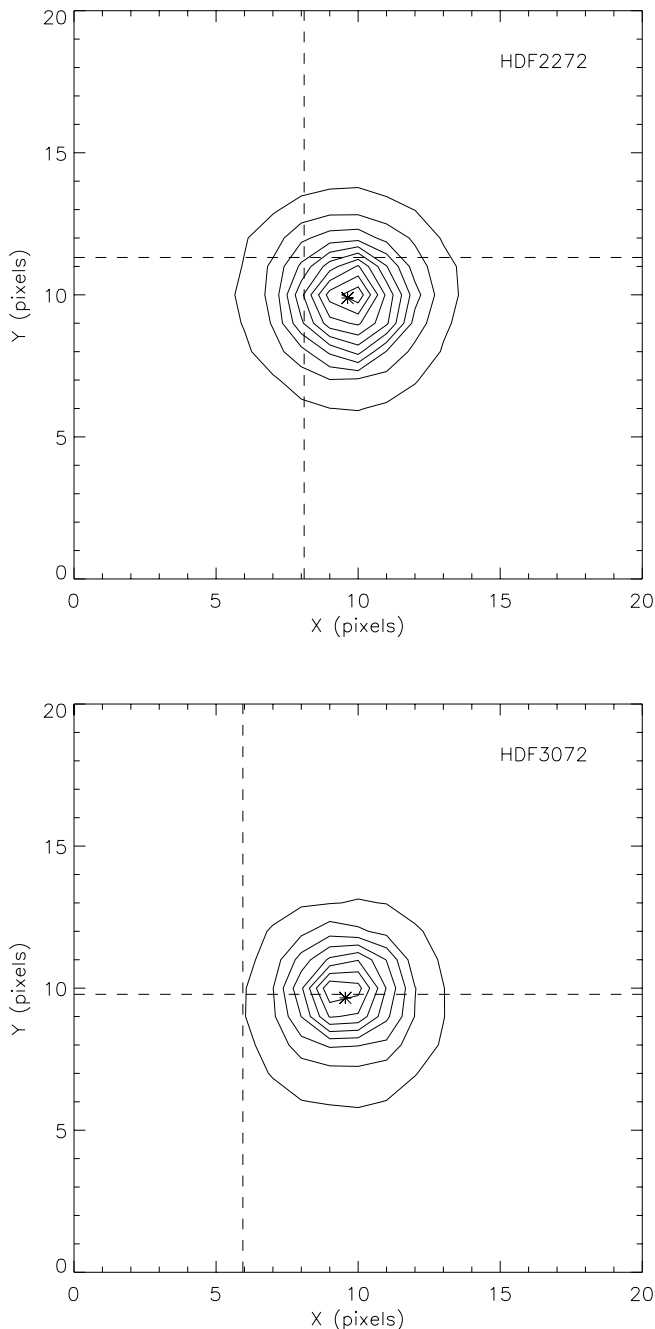
FIG. 1.—Two bright, apparently moving objects. The panels show contour maps and first- and second-epoch positions of the stars HDF 2272 and HDF 3072. The contour maps show the flux distribution around each object (20 × 20 pixels, 0″.6 × 0″.6). Dashed lines cross at the first-epoch position. An asterisk marks the second-epoch position.

STScI. Even with these distortion corrections, however, some distortion remains (Bedin et al. 2003). The effect of the remaining distortion is larger if a global coordinate transformation is used. Instead of performing a global transformation, we have used the IRAF routine GEOMAP to derive a quadratic local transformation for each star, using a surrounding net of several dozen compact objects (isolated, low residuals, and not fuzzy). After mapping the distortions with the GEOMAP package, object coordinates were transformed to the second-epoch positions with the GEOXYTRAN routine.

Figure 1 shows the contour maps for the two bright stars HDF 2272 and HDF 3072. The immediate field around each

object is shown with dashed lines crossing at the first-epoch position. The second-epoch position is marked with an asterisk. This figure shows that SExtractor works very well for bright compact objects, and these two objects are apparently moving. For faint objects, pixel maps are more informative than contour maps. Pixel maps for two faint, possibly moving objects are shown in Figure 2. Solid lines cross at the first-epoch position, and the second-epoch position is marked with a box. Centroiding errors for faint stars are naturally worse; therefore, proper motion errors are larger for the fainter stars.

3. RESULTS

Proper motion measurements are mainly affected by distortion mapping and selection of reference objects. The rms error of the transformations are larger than the positional errors of the objects. In order to check our distortion solution we have used the GEOMAP package with different polynomial terms. We started with no distortion correction and deleted deviant points using a 3 σ rejection algorithm. Rejection of very deviant points is required because our reference objects are compact galaxies and centroiding errors are larger for galaxies. We used quadratic, quadratic with one cross-term, and quadratic with four cross-terms local transformations. For most of the objects, the results from higher order transformations were very similar to the results from the quadratic (with no cross-term) local transformation. This gave us confidence in the stability of our procedure. For two objects, the use of the higher order terms made the distortion solution unstable because of the relative positioning of the reference objects. To be conservative, we adopted the quadratic with no cross-term local transformation for distortion mapping for all of our objects.

Figure 3 shows the differences between second-epoch coordinates and transformed first-epoch coordinates for one of our stars, HDF 1583, and the surrounding 40 reference objects. A 3 σ rejection algorithm is later used to eliminate outliers from the sample. Error bars include positional errors from the SExtractor first- and second-epoch coordinates and the rms error of the transformation. It is clear from this figure that HDF 1583 is statistically well separated from the reference objects, most or all of which are galaxies; it is moving with respect to this external reference frame.

In order to further test our transformations, we have also used all compact objects with positional differences between the two epochs of less than 0.4 pixels to perform a global transformation. We found 377 compact galaxies matching our criteria and fitted a quadratic polynomial to map the distortions. As described above, we have measured proper motions in four to six different ways. Our conservative estimate of the proper motions, their significance (μ/σ), and position angle are given in Table 2, along with the observed range of proper motions from different transformation versions. A comparison of the observed ranges and errors for the proper motion measurements show that the errors are consistent with the variations between fitting techniques. Typical errors in our measurements are ~2.5 mas yr^{-1}. Hence, only those objects having proper motions larger than 5 mas yr^{-1} have significance greater than 2. The bright objects HDF 2272, HDF 2234, HDF 101, HDF 1583, HDF 3072, HDF 2258, and HDF 1481 are definitely moving, and the faint objects HDF 1816 and HDF 774 might be moving.

Star-galaxy confusion becomes worse at faint magnitudes. Only objects 15 σ above the sky level were analyzed by
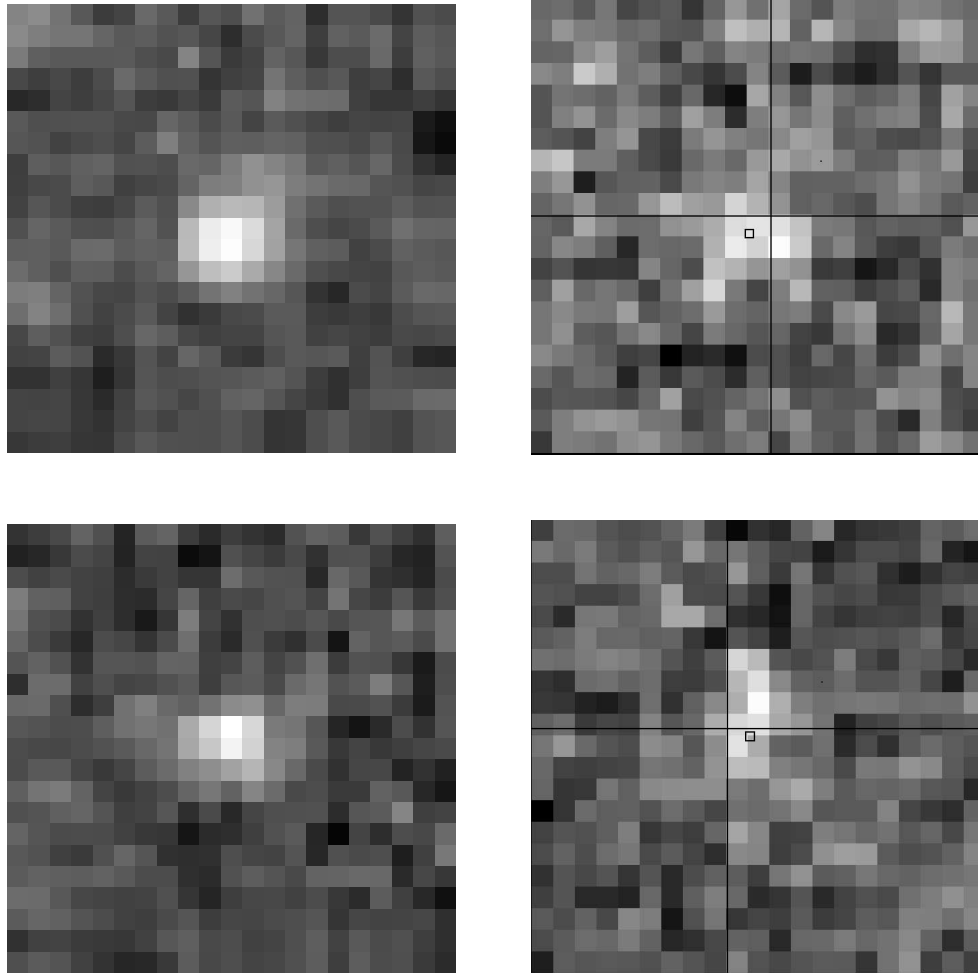
Fig. 2.—Two faint, possibly moving objects. The left panels show pixel maps for the first epoch, and the right panels show pixel maps for the second epoch for HDF 1816 and HDF 774. Solid lines cross at the first-epoch position. The second-epoch position is shown with a box. Images are 20 pixels on a side (0″6).

Mendez & Minniti (2000). Proper motions provide further star-galaxy separation, since anything with a significant proper motion cannot be very distant (e.g., Ibata et al. 1999).

We calculated photometric distances for all objects in our sample assuming that they are either main-sequence stars, white dwarfs, or white dwarfs on the blue hook of the cooling sequence. For a given $V - I$ color, we estimate three absolute magnitudes for each object by linearly interpolating the $V - I$ and M_V relation for main-sequence stars (Table 15.7 of Cox 2000), white dwarfs, and cool white dwarfs (Hansen 1999).

White dwarfs become redder as they cool until the effects of collision-induced absorption due to molecular hydrogen becomes significant below ∼5000 K. The $V - I$ colors for white dwarfs are expected to become bluer for $T_{\rm eff} \lesssim 3500$ K (Hansen 1999; Saumon & Jacobson 1999). Cool white dwarf colors can be quite different in Johnson/Kron-Cousins and the HST filters since H_2 opacity produces sharp flux peaks in the white dwarf spectra. The observed colors of the white dwarfs depend on the transmission peaks of the filters. Richer et al. (2000) calculated the HST colors for white dwarfs using the Holtzmann et al. (1995) bandpasses and the transformations they use to express fluxes in V, R, and I. HDF photometry is calibrated using the Holtzmann et al. (1995) transformations (Mendez & Minniti 2000). Therefore, we used Richer et al. (2000) white dwarf cooling tracks instead of more recent Chabrier et al. (2000b) models. We use the apparent magnitudes

of the objects and the adopted absolute magnitudes to estimate photometric distances.

Proper motion measurements and derived distances can be used to calculate tangential velocities using the equation

$$\mu = \frac{V_{\rm tan}}{4.74d}, \qquad (1)$$

where μ is the proper motion in arcsec yr^{-1}, d is the distance in parsecs, and $V_{\rm tan}$ is the tangential velocity in km s^{-1}. With the assumption that the objects are either main-sequence stars, DA white dwarfs, or cool white dwarfs, derived distances and tangential velocities are given in Table 3. The differences between Chabrier et al. (2000b) and Richer et al. (2000) white dwarf colors are equivalent to absolute magnitude differences of 0–0.5 mag. This corresponds to 0%–25% difference in estimated distances and velocities with an average difference of about 10%.

3.1. Bright Sources ($V \leq 27$)

Mendez & Minniti (2000) analyzed sources brighter than $V = 27$, for which SExtractor gives reliable star-galaxy separation. The same sources have stellarity indices ≥ 0.97 in the GOODS data (Giavalisco et al. 2004), which have better spatial resolution than the original HDF images. The morphology of
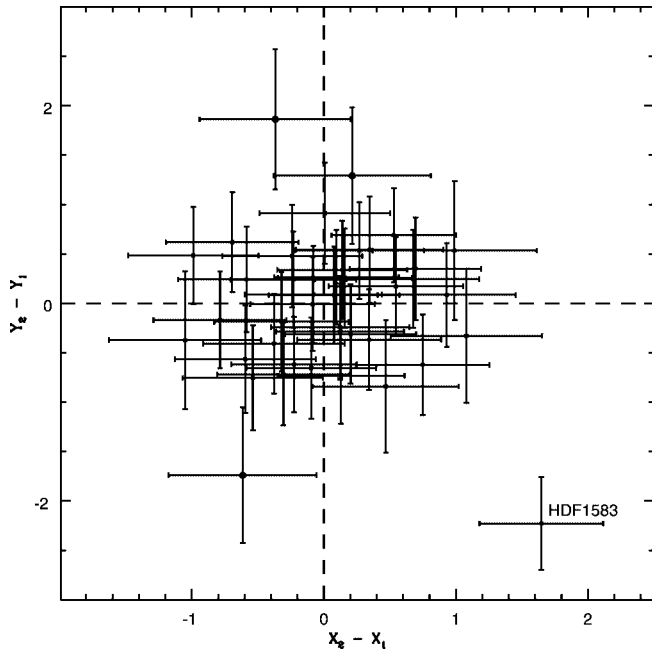
Fig. 3.—Difference between second-epoch coordinates (X_2, Y_2) and transformed first-epoch coordinates (X_1, Y_1) for HDF 1583 and the surrounding reference compact objects. Reference objects that are not included in our transformations are shown as open circles. Error bars include centroiding errors from the first and second epochs, and the rms error of the GEOMAP transformation. HDF 1583 is an example of an object that is clearly exhibiting proper motion.

these sources as pointlike is well supported. HDF 2272, HDF 2234, HDF 101, HDF 1583, HDF 1828, HDF 2134 and HDF 2258 are further confirmed to be stars with Keck LRIS spectroscopy (Cohen et al. 2000).

We have searched the 503 X–ray point sources detected in the 2 ms *Chandra* exposure of the region around the HDF-N called the *Chandra* Deep Field North (Barger et al. 2003) for possible matches with the point sources analyzed here. We did not find any objects matching our objects within a search radius of 0″.5; we could not confirm if we had any quasars among our objects.

A comparison of the distances, tangential velocities, and photometric colors show that HDF 1828, HDF 2134, HDF 2258, HDF 1481, HDF 684, and HDF 3000 are halo main-sequence stars (Table 3). Their $V - I$ colors are too red to be white dwarfs. HDF 2272, HDF 101, HDF 1583, and HDF 1470 can be either main-sequence stars or white dwarfs. Since we are sampling a larger volume for main-sequence stars, these four stars are likely to be main-sequence stars. Cohen et al. (2000) classified HDF 2272 and HDF 1583 as stars showing Mg absorption and Balmer lines, and HDF 2234, HDF 101, HDF 1828, HDF 2134 and HDF 2258 as stars showing TiO or CaH bands.

HDF 2234, HDF 3072, HDF 161, HDF 3031, and HDF 759 would have to be at very large distances and moving with velocities higher than the escape velocity of our Galaxy if they were main-sequence stars. The first 11 objects ($V \leq 26$) in Table 1 are also detected in the Hawaii-HDF-N Survey (Capak et al. 2004), an intensive multicolor (U, B, V, R, I, z, HK) imaging survey of 0.2 deg² centered on the HDF-N. Figure 4

TABLE 2
PROPER MOTIONS

Object	μ (mas yr^{-1})	σ	μ/σ	μ (range)	Position Angle
HDF 2272	8.95	2.48	3.61	8.30–10.09	227.0
HDF 2234	10.05	2.46	4.09	8.67–11.08	298.3
HDF 101	6.03	2.50	2.41	5.00–6.34	238.0
HDF 1583	11.60	2.25	5.17	11.48–11.97	215.3
HDF 1828	2.47	2.06	1.20	1.21–3.08	281.7
HDF 3072	15.47	3.83	4.04	15.40–17.51	268.0
HDF 2134	3.28	2.65	1.24	2.84–4.44	184.4
HDF 2258	8.34	2.92	2.86	8.02–8.86	204.2
HDF 1470	4.06	3.06	1.33	3.40–4.06	230.6
HDF 1481	10.53	2.51	4.19	10.32–11.38	156.1
HDF 161	1.72	1.53	1.12	1.27–2.42	96.5
HDF 684	3.71	2.19	1.69	3.33–4.42	191.0
HDF 3031	1.53	2.68	0.57	1.53–3.76	211.3
HDF 759	1.37	2.56	0.53	0.29–1.73	206.6
HDF 3000	3.66	2.35	1.56	3.43–5.24	230.7
HDF 995	1.24	1.64	0.76	1.21–1.44	190.5
HDF 1022	3.27	3.06	1.07	2.19–4.14	251.7
HDF 861	2.22	2.93	0.76	1.56–2.22	160.8
HDF 1705	3.64	3.00	1.21	1.83–5.53	235.1
HDF 2729	3.45	1.99	1.73	2.88–3.78	106.6
HDF 2217	2.01	2.79	0.72	1.78–2.86	358.0
HDF 806	1.15	2.91	0.40	0.88–2.36	90.4
HDF 1135	3.45	2.00	1.73	3.45–4.11	297.6
HDF 2991	3.77	3.28	1.15	2.84–3.86	36.6
HDF 1288	3.55	2.89	1.23	2.17–4.25	206.1
HDF 723	2.76	2.42	1.14	2.32–3.69	98.4
HDF 1816	5.49	1.89	2.91	4.77–6.30	129.2
HDF 1039	3.13	2.50	1.25	2.28–4.44	200.8
HDF 774	4.80	2.38	2.02	3.56–5.22	251.3

Object	d (MS)	σ_d (MS)	$V_{\tan}$ (MS)	σ_v (MS)	d (WD)	σ_d (WD)	$V_{\tan}$ (WD)	σ_v (WD)	d (CWD)	σ_d (CWD)	$V_{\tan}$ (CWD)	σ_v (CWD)
HDF 2272	6194	141	263	73	100.0	1.0	4.24	1.18	29.65	0.04	1.26	0.35
HDF 2234	61094	2339	2911	720	554.6	7.6	26.43	6.46	43.65	0.02	2.08	0.51
HDF 101	11803	240	338	140	189.7	2.6	5.42	2.25	66.68	0.24	1.91	0.79
HDF 1583	10965	177	603	117	115.3	2.4	6.34	1.23	...	...	...	...
HDF 1828	10375	167	122	101	...	...	...	...	...	...	...	...
HDF 3072	34674	630	2542	631	505.8	9.6	37.09	9.20	264.24	0.64	19.37	4.79
HDF 2134	11015	178	172	139	...	...	...	...	...	...	...	...
HDF 2258	7482	174	296	104	...	...	...	...	...	...	...	...
HDF 1470	44874	1044	864	651	472.1	7.6	9.09	6.85	...	...	...	...
HDF 1481	25119	553	1254	301	...	...	...	...	...	...	...	...
HDF 161	214783	27485	1748	1575	2228.4	74.6	18.13	16.19	428.55	1.13	3.49	3.11
HDF 684	58614	2236	1030	610	...	...	...	...	...	...	...	...
HDF 3031	599791	55449	4359	7627	5128.6	513.7	37.27	65.23	594.29	1.65	4.32	7.55
HDF 759	628058	58264	4079	7635	5248.1	566.2	34.08	63.83	639.73	1.80	4.15	7.77
HDF 3000	15276	895	265	171	...	...	...	...	...	...	...	...
HDF 995	580764	257760	3420	4756	5728.0	430.5	33.73	44.53	779.83	2.26	4.59	6.05
HDF 1022	1.39E06	332181	21556	20807	12416.5	2541.7	192.56	184.34	1132.4	6.92	17.56	16.42
HDF 861	2.28E06	1.65E06	24031	36146	19588.4	5296.6	206.46	277.90	1153.45	7.06	12.16	16.03
HDF 1705	1.22E06	313129	21039	18175	10232.9	2995.5	176.47	154.46	1247.38	11.59	21.51	17.74
HDF 2729	812831	302641	13276	9129	8053.8	1321.2	131.54	79.05	1386.76	13.07	22.65	13.10
HDF 2217	1.55E06	546469	14754	21179	13740.4	3411.5	130.79	184.87	1348.96	16.89	12.84	17.87
HDF 806	1.02E06	134633	5564	14085	10139.1	2030.9	55.30	140.26	1555.97	19.87	8.49	21.46
HDF 1135	326588	111650	5341	3589	5128.6	1655.4	83.87	55.56	1995.26	151.44	32.63	19.04
HDF 2991	2.06E06	780649	36825	34953	18793.2	6184.8	335.95	312.56	1577.61	20.18	28.20	24.54
HDF 1288	4.79E06	6.39E06	80608	125961	30338.9	7070.9	510.55	432.17	1570.36	15.06	26.43	21.51
HDF 723	508159	281257	6652	6889	7585.8	1206.8	99.30	88.34	1923.09	75.78	25.17	22.06
HDF 1816	1.89E06	717666	49213	25202	15995.6	7053.9	416.51	232.85	1896.71	88.67	49.39	17.13
HDF 1039	...	...	...	...	...	...	...	...	...	...	...	...
HDF 774	3.89E06	4.61E06	88595	113808	31477.5	9203.1	716.90	412.59	1786.49	17.43	40.69	20.17

Note.—Assuming that the object is either a main-sequence star (MS), a white dwarf (WD), or a very cool white dwarf (CWD, $T_{\rm eff} \lesssim 3500$ K). Distances are in parsecs, and velocities are in km s^{-1}.
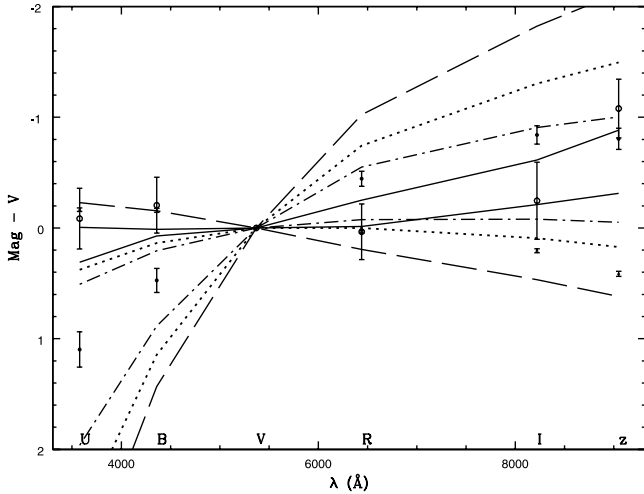
Fig. 4.—Normalized *UBVRIz* magnitudes for HDF 2234 (*filled triangles*), HDF 3072 (*filled circles*), and HDF 161 (*open circles*). The observed magnitudes are normalized at *V*. The colors for a 15,000 and 3000 K blackbody are shown as long-dashed lines. Dashed-dotted lines represent two DA white dwarf models (7000 and 3500 K), and dotted lines represent two DB white dwarf models (8000 and 3500 K; D. Saumon 2003, private communication). Also shown are colors for a QSO at $z = 0.3$ (*upper solid line*) and another at $z = 0.7$ (*lower solid line*).

Fig. 5.—Keck/DEIMOS (uncalibrated) spectrum of HDF 2234 observed by the Team Keck Treasury Redshift Survey. The spectrum is smoothed with a 5 pixel–wide boxcar. Instrument efficiency for the blocking filter used for the observations is shown as a dotted line. The broad feature at ~5400 Å is due to the instrument efficiency, and the feature at 6890 Å is the atmospheric *B* band. The only detectable feature is Hα.

shows normalized *UBVRIz* magnitudes for HDF 2234 (*filled triangles*), HDF 3072 (*filled circles*), and HDF 161 (*open circles*) along with colors for a 15,000 and 3000 K blackbody (*long-dashed lines*). The observed magnitudes are normalized at *V*. Dashed-dotted lines represent two DA white dwarf models (7000 and 3500 K), and dotted lines represent two DB white dwarf models (8000 and 3500 K; D. Saumon 2003, private communication). Our simulations for a QSO at $z = 0.3$ (*upper solid line*) and another at $z = 0.7$ (*lower solid line*) are also shown. We have used the composite quasar spectra from the Sloan Digital Sky Survey (Vanden Berk et al. 2001) to simulate the colors for quasars. Plotting all of the normalized magnitudes in the same plot is an efficient way of presenting all of the data; it is similar to plotting low-resolution spectroscopy.

A comparison of the observed colors of HDF 2234 with the models shows that it is hotter than 10,000 K. J. Cohen kindly provided us the Keck/LRIS spectrum for HDF 2234. The same object is also observed by the Team Keck Treasury Redshift Survey (Wirth et al. 2004) who made their data publicly available. Figure 5 shows the uncalibrated spectrum of HDF 2234 observed by the Team Keck Treasury Redshift Survey. The object shows Hα at its rest wavelength; it is a star in our Galaxy. Although Cohen et al. (2000) classified this object as a late-type star showing CaH or TiO, its colors indicate that HDF 2234 is too hot to show CaH and/or TiO. Absence of Hβ and Mg absorption eliminates the possibility of the object being a main-sequence star. The broad feature at ~5400 Å might be due to the efficiency of the instrument+blocking filter combination, and the 6890 Å feature is the atmospheric *B* band. The star could be a cool DA white dwarf showing only Hα. However, the colors indicate that this should be a white dwarf hotter than 10,000 K, which is inconsistent with such weak H lines, unless the star is a DC white dwarf at a position just too cool to show He I (11,000 K), but then Hα alone cannot be explained. The nature of this object remains ambiguous at this time. Follow-up spectroscopy in the blue is needed to confirm that this object is a white dwarf.
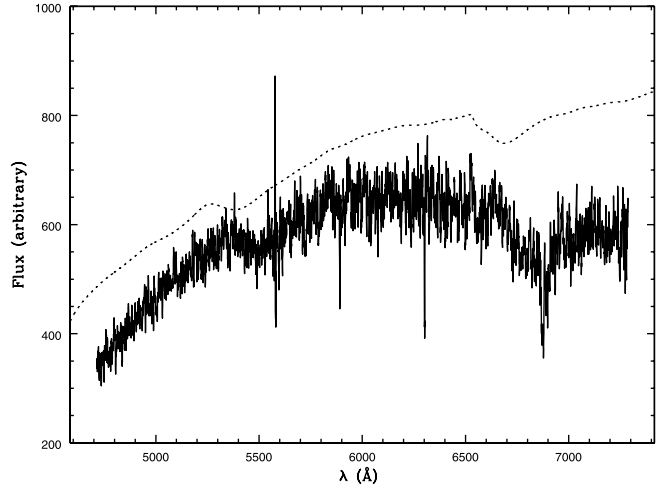
HDF 3072 displays even higher apparent proper motion than HDF 2234, 15.47 ± 3.83 mas yr^{-1}. Its colors and implied distance and velocity are consistent with a ~4500 K white dwarf at $d \approx 500$ pc.

The faint blue objects in Mendez & Minniti (2000) are HDF 684, HDF 161, HDF 3031, HDF 759, and HDF 995. We have classified HDF 684 as a main-sequence star (see above). The rest of the faint blue objects, HDF 161, HDF 3031, HDF 759, and HDF 995, do not seem to exhibit any proper motion. HDF 161 was near the detection limit of the Hawaii-HDF-N, and the other three objects are not detected in the Hawaii-HDF-N. Figure 4 shows that HDF 161 (*open circles*) exhibits a near-infrared excess; it is consistent with being a QSO under the given photometric uncertainties. Therefore, we believe that HDF 161, HDF 3031, and HDF 759 are probably active galactic nuclei (AGNs). These objects cannot be low-mass main-sequence stars, brown dwarfs, or free-floating planets because of their blue colors (see Chabrier et al. 2000a). Also, they cannot be comets or asteroids in our solar system because of their small proper motions (A. Cochran 2004, private communication). Because of the large errors in the distance and velocity for HDF 995, its nature is unclear.

3.2. *Faint Sources* ($27 \geq V \geq 29$)

Star-galaxy separation becomes ambiguous below $V \approx 27$. Proper motions can be used to identify stars fainter than 27th magnitude since a moving object has to be in our Galaxy. We find that only two of the objects in our sample, HDF 1816 and HDF 774, have significant movement. These two objects are most likely Galactic white dwarfs. The rest of the faint objects do not show any significant movement ($\mu/\sigma \leq 2$). For these objects, distances and velocities are consistent with halo white dwarfs or extragalactic sources. Mendez & Minniti (2000) found 566 extragalactic sources in the same magnitude and color range as the five faint blue sources that are brighter than 27th magnitude. The ratio of the number of extragalactic objects to the number of stars increases at fainter magnitudes. Therefore, we believe that faint sources, with no significant apparent proper motion, are extragalactic objects.
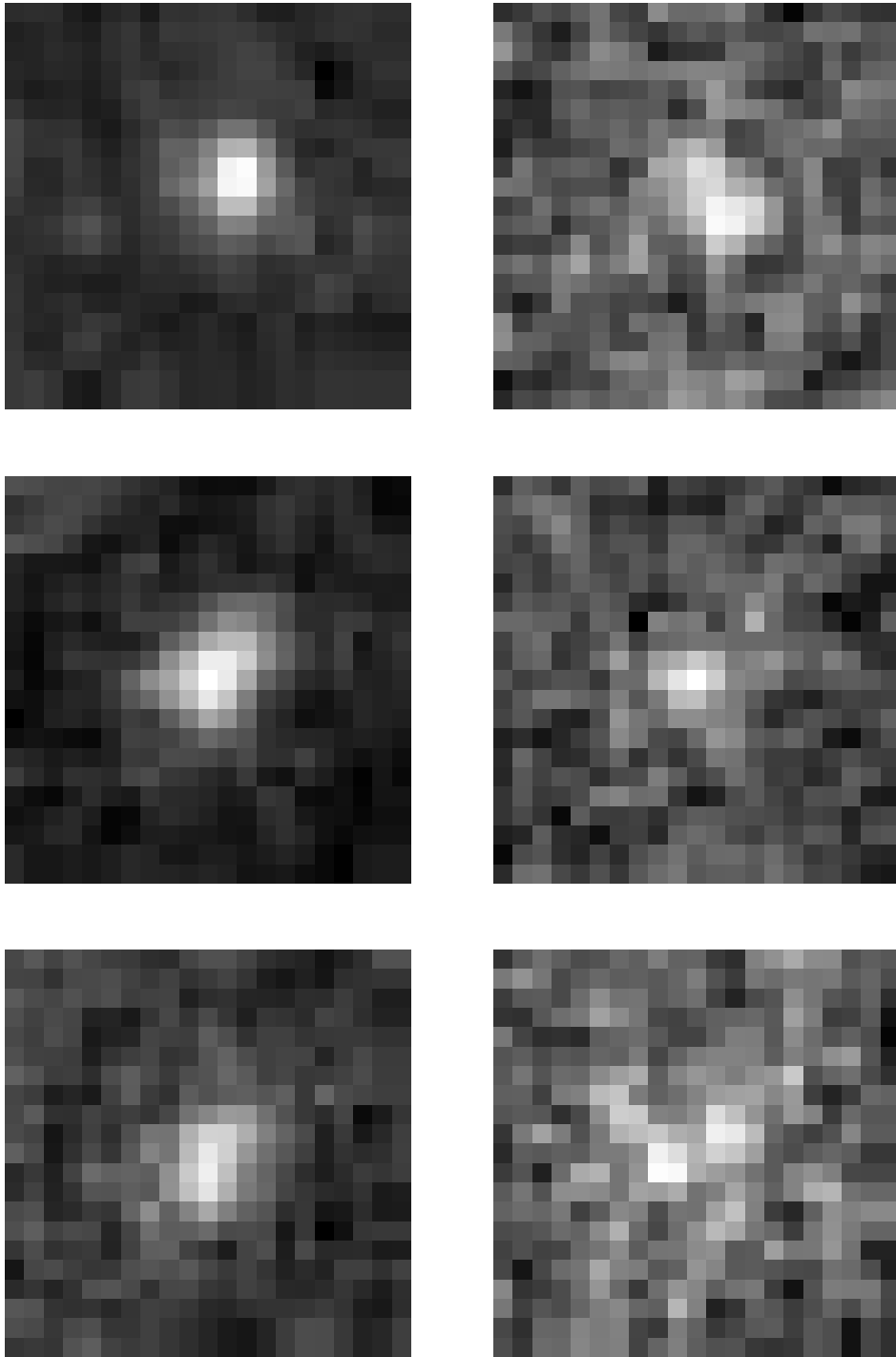
Fig. 6.—Pixel maps for three of the Ibata et al. (1999) objects, HDF 2837, HDF 2952, and HDF 574 with stellarity indices of 0.68, 0.07, and 0.11, respectively. Visual inspection of the images further confirms that these are extended objects. Note that we have not measured proper motions for these objects.

3.3. *Ibata et al. (1999) Objects*

Ibata et al. (1999) obtained second-epoch exposures of the HDF in 1997 and derived proper motions using a 2 yr baseline. They found that two blue, faint objects displayed proper motions ~25 mas yr⁻¹ and three other stars at the detection limit of the second-epoch observations might be moving. Third-epoch data on these objects showed that these objects are not moving (R. Ibata 2003, private communication; Richer et al. 2001).

Two of the objects in the Ibata et al. (1999) sample are in common with Mendez & Minniti (2000) objects. These two objects, HDF 806 and HDF 1816, have stellarities larger than 0.9 and are therefore classified as stars by SExtractor. Stellarity is the probability of an object being a point source (stellarity = 1) or an extended object (stellarity = 0) assigned by SExtractor. Mendez & Minniti (2002) found that all objects with stellarity less than 0.85 are clearly extended and used a conservative cut at stellarity greater than 0.90 to identify point sources. We find that HDF 806 and HDF 1816 have proper motions of 1.15 ± 2.91 mas yr⁻¹ and 5.49 ± 1.89 mas yr⁻¹, respectively. The other three objects are classified as galaxies by the SExtractor. Visual inspection of the first- and second-epoch images (Fig. 6) shows that these three objects are extended and clearly not stars. We conclude that three of the objects (2-766, 4-141, 4-551) in the Ibata et al. (1999) sample are galaxies, HDF 806 (2-455) is not moving, and HDF 1816 (4-492) is probably moving (2.9 σ significance).

4. DISCUSSION

The nature of the faint blue objects in the HDF may be crucial to understanding the contribution of low-luminosity halo white dwarfs to microlensing events and the dark matter content of the Galaxy. Apparent proper motions for five faint blue objects (Ibata et al. 1999) was enough to explain the entire missing mass in the halo of the Milky Way. Mendez & Minniti (2000) claimed that the faint blue objects are white dwarf stars located at heliocentric distances of up to 2 kpc and belong to the Galactic halo. They found a local halo white dwarf mass density of 4.64×10^{-3} $M_\odot$ pc⁻³, which would account for about 30%–50% of the dark matter in the Galaxy.

With the advantage of a 7 yr baseline, we are able to place better limits on the proper motion measurements of the faint blue objects. Using the proper motion information, we also derived distances and tangential velocities for these objects. Figure 7 shows the tangential velocities and distances for objects brighter than $V \approx 27$ assuming that they are main-sequence stars or DA white dwarfs. All of the main-sequence stars exhibit halo kinematics and distances, whereas all of the likely white dwarfs exhibit disk kinematics and distances.

Following Gilmore et al. (1989; see also von Hippel & Bothun 1990), we use the analytical form of the density profile for the thin disk and thick disk

$$\frac{\nu_0(z)}{\nu_0(0)} = 0.96\ e^{-z/250\,\mathrm{pc}} + 0.04\ e^{-z/1000\,\mathrm{pc}} \qquad (2)$$

with a local normalization of 0.11 $M_\odot$ pc⁻³ (Pham 1997). We use the form

$$\nu_{\mathrm{halo}}(r) \propto \frac{\exp\left[-7.669\,(R/R_e)^{(1/4)}\right]}{(R/R_e)^{(7/8)}} \qquad (3)$$
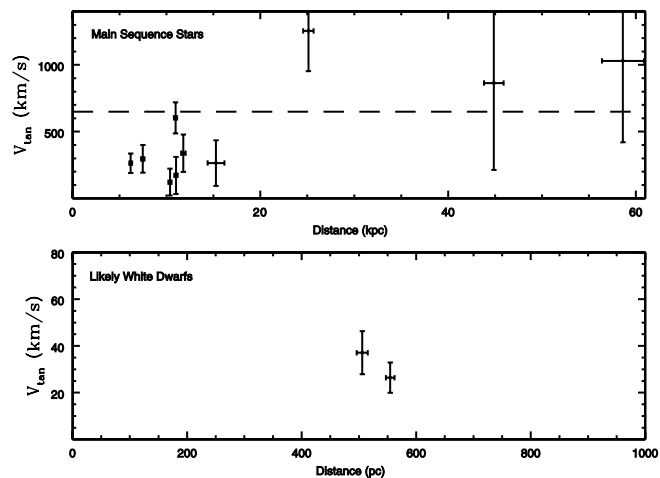

Fig. 7.—Tangential velocities and distances for main-sequence stars (*top panel*) and likely white dwarfs (*bottom panel*) brighter than 27th magnitude. The dashed line marks the upper bound for the escape velocity from the Milky Way (650 km s⁻¹; Leonard & Tremaine 1990; Meillon et al. 1997). All of the main-sequence stars have halo properties, whereas the probable white dwarfs have disk properties.

for the halo (Young 1976), where R is the distance from the Galactic center, and R_e is the scale factor. R is related to the distance r from the observer to a star by

$$R^2 = R_0^2 + r^2 - 2rR_0 \cos b \cos l, \qquad (4)$$

where R_0 is the solar galactocentric distance, and b and l are the Galactic coordinates for the HDF-N. We use $R_0 = 7.8$ kpc (Gilmore et al. 1989), $R_e = 2.7$ kpc (de Vaucouleurs & Pence 1978), and a local normalization for the halo of $(1/800) \times 0.11$ $M_\odot$ pc⁻³ (Chen et al. 2001; Gilmore et al. 1989). Using equations (2), (3), and (4), we calculated the expected number of stars in the HDF. We expect to find two thin disk, three thick disk, and 11 halo objects in the HDF-N.

We have also used Reid & Majewski (1993) star count models to predict the number of stars in the HDF-N. We found that two thin disk, four thick disk, and 14 halo objects are expected in the HDF-N. Both simple analytical models and more sophisticated star count models, when extrapolated to the photometric depth of the HDF, predict similar number of stars (16–20) in the HDF-N.

There are 14 stars brighter than $V = 27$ and 17 objects fainter than $V = 27$ classified as stars by SExtractor. The observed number of stars and the predictions of star count models are in good agreement for $V \lesssim 27$ (see also Mendez et al. 1996 and Mendez & Minniti 2000). On the other hand, there seems to be an excess of point sources in the HDF-N for $V \gtrsim 27$. Unfortunately, SExtractor classification cannot be trusted at these magnitudes. Furthermore, we did not detect significant proper motion for all but two of these objects. The two faint, possibly moving objects, HDF 774 and HDF 1816, may be halo white dwarfs. One of the problems with any analysis using these objects is that the observations are beyond the completeness limit, and any calculation based on them is subject to a significant completeness correction. The rest of the objects fainter than $V = 27$ are probably extragalactic objects (see § 3.2).

The five faint blue objects analyzed by Mendez & Minniti (2000) do not exhibit any significant proper motion; they are not halo white dwarfs. These objects do not account for the MACHO optical depth and are not the source of the Galactic

dark matter. Their stellar nature is not confirmed either. The colors of HDF 161 are consistent with our QSO simulations. The faint blue objects may be distant AGNs.

Holberg et al. (2002) used a local sample of white dwarfs complete out to 13 pc and found the local mass density of white dwarf stars to be $(3.4 \pm 0.5) \times 10^{-3}$ $M_\odot$ pc^{-3}. Using this normalization factor in equations (2) and (3), we estimate the expected number of white dwarfs in the HDF. We expect to find 0.05 disk white dwarfs, 0.09 thick disk white dwarfs, and 0.33 halo white dwarfs in the HDF-N. We have also used Reid & Majewski (1993) star count models to predict the number of white dwarfs in the HDF. The results are roughly consistent: 0.10 disk, 0.25 thick disk, and 0.5 halo white dwarfs are expected.

We have discovered two likely white dwarfs, HDF 2234 and HDF 3072, brighter than $V = 27$ in the HDF-N. They are located at distances of $\sim$500 pc and have tangential velocities $\sim$30 km s^{-1}. Their kinematic properties are consistent with being thin disk or thick disk objects (see Table 3 and Fig. 7). The expected number of thin disk+thick disk white dwarfs is found to be 0.14–0.35. We have found 6–14 times more disk white dwarfs in the HDF-N than expected from the models. Assuming Poisson statistics, the probability of finding two white dwarfs is 1% if the expected number of white dwarfs is 0.14 and 4% if the expected number of white dwarfs is 0.35. The number of disk+thick disk white dwarfs may be substantially underestimated. Because of small number statistics, however, this statement is only a 2–3 σ result and it heavily depends on the fact that HDF 2234 and HDF 3072 are white dwarfs. Follow-up spectroscopy of these two objects is needed to confirm this result.

Mendez & Minniti (2000) have found 22 Galactic stars and 10 faint blue objects in the HDF-S. A natural test to check the space density of disk and halo white dwarfs would be to obtain second-epoch observations of the HDF-S to find high proper motion objects. Also, the *HST*/ACS Ultra-Deep Field observations of the *Chandra* Deep Field–South will be useful to search for faint blue objects at fainter magnitudes and to improve the morphological classification of these objects at brighter magnitudes. The Ultra-Deep Field will be $\sim$1.5 mag deeper than the HDF and HDF-S (Beckwith et al. 2003).

REFERENCES

Afonso, C., et al. 2003, A&A, 400, 951
Alcock, C., et al. 1997, ApJ, 486, 697
———. 2000, ApJ, 542, 281
Anderson, J., & King, I. R. 2000, PASP, 112, 1360
Barger, A. J., et al. 2003, AJ, 126, 632
Beckwith, S. V. W., et al. 2003, BAAS, 202, 1705
Bedin, L. R., Piotto, G., King, I. R., & Anderson, J. 2003, AJ, 126, 247
Bergeron, P. 2003, ApJ, 586, 201
Bertin, E., & Arnouts, S. 1996, A&AS, 117, 393
Capak, P., et al. 2004, AJ, 127, 180
Casertano, S., et al. 2000, AJ, 120, 2747
Chabrier, G., Baraffe, I., Allard, F., & Hauschildt, P. 2000a, ApJ, 542, 464
Chabrier, G., Brassard, P., Fontaine, G., & Saumon, D. 2000b, ApJ, 543, 216
Chen, B., et al. 2001, ApJ, 553, 184
Cohen, J. G., et al. 2000, ApJ, 538, 29
Cox, A., ed. 2000, Allen's Astrophysical Quantities (4th ed.; New York: Springer)
de Vaucouleurs, G., & Pence, W. D. 1978, AJ, 83, 1163
Flynn, C., Gould, A., & Bahcall, J. N. 1996, ApJ, 466, L55
Giavalisco, M., et al. 2003, BAAS, 202, 1703
Gilmore, G., King, I. R., & van der Kruit, P. C. 1989, in The Milky Way as a Galaxy, ed. R. Buser and I. R. King (Saas-Fée Advanced Course 19; Mill Valley: University Science Books)
Hansen, B. M. S. 1999, ApJ, 520, 680
Holberg, J. B., Oswalt, T. D., & Sion, E. M. 2002, ApJ, 571, 512
Holtzman, J. A., Burrows, C. J., Casertano, S., Hester, J. J., Trauger, J. T., Watson, A. M., & Worthey, G. 1995, PASP, 107, 165
Ibata, R.A., Irwin, M., Bienaymé, O., Scholz, R., & Guibert, J. 2000, ApJ, 532, L41

Ibata, R. A., Richer, H. B., Gilliland, R. L., & Scott, D. 1999, ApJ, 524, L95
Kawaler, S. D. 1996, ApJ, 467, L61
Leonard, P. J. T., & Tremaine, S. 1990, ApJ, 353, 486
Meillon, L., Crifo, F., Gomez, A. E., Udry, S., & Mayor, M. 1997, in Proc. ESA Symp. *Hipparcos*—Venice '97, ed. B. Battrick (ESA SP-402; Noordwijk: ESA), 591
Mendez, R. A. 2002, A&A, 395, 779
Mendez, R. A., & Minniti, D. 2000, ApJ, 529, 911
Mendez, R. A., Minniti, D., de Marchi, G., Baker, A., & Couch, W. J. 1996, MNRAS, 283, 666
Oppenheimer, B. R., Hambly, N. C., Digby, A. P., Hodgkin, S. T., & Saumon, D. 2001, Science, 292, 698
Pham, H. A. 1997, in Proc. ESA Symp. *Hipparcos*—Venice '97, ed. B. Battrick (ESA SP-402; Noordwijk: ESA), 559
Reid, N., & Majewski, S. R. 1993, ApJ, 409, 635
Reid, I. N., Sahu, K. C., & Hawley, S. L. 2001, ApJ, 559, 942
Reyle, C., Robin, A. C., & Creze, M. 2001, A&A, 378, L53
Richer, H. B., Hansen, B. M. S., Limongi, M., Chieffi, A., Straniero, O., & Fahlman, G. G. 2000, ApJ, 529, 318
Richer, H. B., et al. 2001, preprint (astro-ph/0107079)
Saumon, D., & Jacobson, S. B. 1999, ApJ, 511, L107
Udalski, A., Szymanski, M., Kaluzny, J., Kubiak, M., & Mateo, M. 1992, Acta Astron., 42, 253
Vanden Berk, D. E., et al. 2001, AJ, 122, 549
von Hippel, T., & Bothun, G. 1990, AJ, 100, 403
Williams, R. E., et al. 1996, AJ, 112, 1335
Wirth, G. D., et al. 2004, preprint (astro-ph/0401353)
Young, P. J. 1976, AJ, 81, 807